Vacuum 184 (2021) 109979

Contents lists available at ScienceDirect

Vacuum

journal homepage: www.elsevier.com/locate/vacuum

Neutral tritium gas reduction in the KATRIN differential pumping sections

A. Marsteller [a,*], B. Bornschein [a], L. Bornschein [b], G. Drexlin [c], F. Friedel [b], R. Gehring [d], S. Grohmann [e], R. Gumbsheimer [b], M. Hackenjos [h,1], A. Jansen [b], A. Kosmider [g,1], L. La Cascio [c], S. Lichter [b], K. Müller [b], F. Priester [a], R. Rinderspacher [b], M. Röllig [a], C. Röttele [a], F. Sharipov [f], M. Sturm [a], S. Welte [a], J. Wolf [c]

[a] Institute for Astroparticle Physics, Tritium Laboratory Karlsruhe(IAP-TLK), Karlsruhe Institute of Technology (KIT), Hermann-von-Helmholtz-Platz 1, 76344 Eggenstein-Leopoldshafen, Germany
[b] Institute for Astroparticle Physics (IAP), Karlsruhe Institute of Technology (KIT), Hermann-von-Helmholtz-Platz 1, 76344 Eggenstein-Leopoldshafen, Germany
[c] Institute of Experimental Particle Physics (ETP), Karlsruhe Institute of Technology (KIT), Wolfgang-Gaede-Str. 1, 76131 Karlsruhe, Germany
[d] Institute for Technical Physics (ITEP), Karlsruhe Institute of Technology (KIT), Hermann-von-Helmholtz-Platz 1, 76344 Eggenstein-Leopoldshafen, Germany
[e] Institute of Technical Thermodynamics and Refrigeration (ITTK), Karlsruhe Institute of Technology (KIT), Engler-Bunte-Ring 21, 76131 Karlsruhe, Germany
[f] Departamento de Física, Universidade Federal do Paraná, Caixa Postal 19044, 81531-980, Curitiba, Brazil
[g] Helmholtz Association Berlin Office, Anna-Louisa-Karsch-Str. 2 10178, Berlin, Germany
[h] Karlsruhe Institute of Technology (KIT), Hermann-von-Helmholtz-Platz 1, 76344, Eggenstein-Leopoldshafen, Germany

ARTICLE INFO

Keywords:
KATRIN experiment
Vacuum measurement
Tritium
Gas flow
Pumping speed
TPMC simulation

ABSTRACT

The KArlsruhe TRItium Neutrino experiment (KATRIN) aims to measure the effective electron anti-neutrino mass with an unprecedented sensitivity of 0.2 eV/c^2, using β-electrons from tritium decay. The electrons are guided magnetically by a system of superconducting magnets through a vacuum beamline from the windowless gaseous tritium source through differential and cryogenic pumping sections to a high resolution spectrometer and a segmented silicon pin detector. At the same time tritium gas has to be prevented from entering the spectrometer. Therefore, the pumping sections have to reduce the tritium flow by more than 14 orders of magnitude. This paper describes the measurement of the reduction factor of the differential pumping section performed with high purity tritium gas during the first measurement campaigns of the KATRIN experiment. The reduction factor results are compared with previously performed simulations, as well as the stringent requirements of the KATRIN experiment.

1. Introduction

Neutrinos are the lightest and most abundant of the known massive elementary particles in the universe. They played a crucial role in the evolution of large-scale structures [1] in the early universe. Although, it is established since the 1990s that the different neutrino flavor species are related to individual compositions of the neutrino mass eigenstates [2], of which at least two are non-vanishing, the absolute values are still unknown. At present, upper limits are available from cosmic surveys, such as the cosmic microwave background [3], and from direct neutrino mass searches using β-decays [4,5]. Neutrino oscillation experiments, which are only sensitive to the difference between the neutrino mass-squared, can provide lower limits [6]. The determination of the absolute neutrino mass value is still one of the most crucial questions in particle and astroparticle physics.

The Karlsruhe Tritium Neutrino Experiment (KATRIN), operated at the Karlsruhe Institute of Technology (KIT), is currently the most sensitive experiment to determine the neutrino mass from the precise measurement of the kinematics of tritium-β-decay [5] with a design sensitivity of 0.2 eV/c^2 [7]. A non-vanishing neutrino mass would slightly change the shape of the β-spectrum close the endpoint at 18.6 keV. After the commissioning of KATRIN with deuterium measurements in autumn 2017 [8], the first operation with low amounts of radioactive tritium started in spring 2018 [9]. The search for the neutrino mass with an increased tritium flow started in 2019 [5].

The 70 m long KATRIN apparatus comprises two parts (see Fig. 1): the tritium *source and transport section* (STS) located inside the Tritium Laboratory Karlsruhe (TLK) and the tritium-free *spectrometer and detector section* (SDS) located in an adjacent building [10]. The STS

* Corresponding author.
E-mail address: alexander.marsteller@kit.edu (A. Marsteller).
[1] No longer affiliated with KIT, formerly Institute for Nuclear Physics (IKP), Karlsruhe Institute of Technology (KIT).

https://doi.org/10.1016/j.vacuum.2020.109979
Received 21 September 2020; Received in revised form 9 November 2020; Accepted 1 December 2020
Available online 8 December 2020

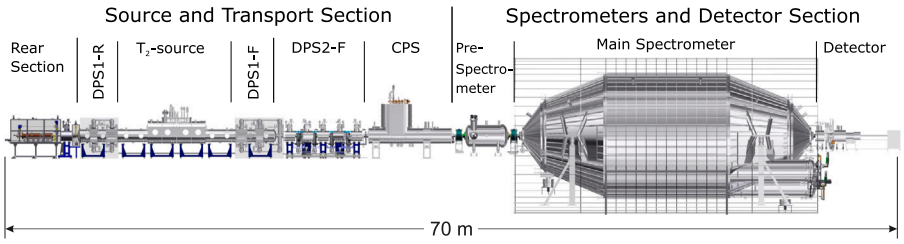

Fig. 1. Overview of the KATRIN beam line.

consists of the *windowless gaseous tritium source* (WGTS) cryostat, followed in downstream direction (towards SDS) by the *transport and pumping section*, and upstream by the *rear section*, which is part of the calibration and monitoring system (CMS). Inside the WGTS beam tube tritium decays to ^{3}He, isotropically emitting electrons and electron-anti-neutrinos. While the neutrinos leave the beam tube without further interaction, the electrons are guided adiabatically by strong magnetic fields along the 40 m long STS-beamline. Half of the electrons travel downstream to the SDS, where their energy is measured by an electrostatic spectrometer (MAC-E filter [11]) with ultra-high precision (1 eV at 20 keV). Virtually all remaining tritium gas in the beam tube is pumped out in the *transport and pumping section*, before it can reach the *spectrometer section*, where otherwise it would increase the background rate of the measurement. Since only 2×10^{-13} of all β-electrons have kinetic energies in the last eV below the endpoint of the spectrum, a low background rate is necessary to reach the target sensitivity. Therefore, the initial tritium flow into the WGTS of 1.8 mbar l s^{-1} (here and in the following referenced to 0 °C) has to be reduced by at least 14 orders of magnitude, before reaching the SDS.

An essential part of the STS is the KATRIN Loop System shown in Fig. 2, which incorporates the pumping systems. It provides a closed inner loop for the ultra-pure and pressure stabilized tritium circulation through the beam tube inside the WGTS cryostat. Simultaneously, the outer loop serves as interlink to the tritium infrastructure of the TLK, where impure tritium gas is cleaned and stored. The transport and pumping section comprises two components. First, the *differential pumping section* (DPS) employs a chain of turbo molecular pumps (TMP), as shown in Fig. 2. The TMPs reduce the flow by 7 orders of magnitude. Details are described in the next section. For lower pressures, mechanical pumping becomes inefficient. Therefore, the second part is a *cryogenic pumping section* (CPS), which cryosorbs the remaining tritium molecules on a 3 K to 4 K cold argon frost layer [12,13]. The Ar frost layer is regenerated regularly, before the accumulated tritium exceeds a maximum activity of 3.7×10^{10} Bq (=1 Ci), as required by radioactive safety considerations. With the nominal tritium flow into the WGTS and the projected flow reduction by the DPS, this limit would be reached after about 60 days. A longer time between regenerations of the CPS increases the possible uptime of the KATRIN experiment. Therefore, an accurate assessment of the actual flow reduction by the DPS is important.

This paper is focused on the reduction of the neutral tritium flow rate along the beamline by the differential pumping section, between the inlet into the beam tube at the center of the WGTS to the entrance of the CPS. The overall performance of the differential pumping system of KATRIN was checked during commissioning with deuterium gas, before admitting tritium into the system. The result has been confirmed during the first tritium measurement in 2018 with 1% DT in deuterium [9]. However, these measurements allow only a rough estimate of the actual tritium reduction efficiency, due to different effective pumping speeds for DT and T_2. The decay rate of DT in the recovered gas after regenerating the Ar frost was used in the second measurement to determine the amount of gas accumulated in the CPS. The ratio between the accumulated gas and the integrated gas flow into the WGTS provides a measure for the reduction factor of the DPS. However, the small admixture of DT introduced a large statistical uncertainty. In 2019, the first KATRIN measurements (KNM1: Mar. 27–May 09, 2019 [5], KNM2: Sep. 27–Nov. 14, 2019) with high tritium concentration (>97%, remainder H and D) were performed, enabling the accurate determination of the DPS reduction factor for tritium. The results are presented in Section 3 and compared to simulations [14] described in the next section.

2. The differential pumping sections of KATRIN

2.1. Description of the differential pumping section

The tritium loop system is distributed along the 40 m long KATRIN STS beam line and interconnects the beam line segments with each other and the TLK infrastructure [15,16]. As shown in Fig. 2, it consists of the "Inner Loop" (IL) and "Outer Loop" (OL). Components of interest for this paper are:

- *Windowless Gaseous Tritium Source (WGTS):* The source of β-electrons in KATRIN is a gas column of tritium in a 10 m long beam tube with 90 mm diameter. In order to achieve the high statistics required for KATRIN, 1.8 mbar l s^{-1} (40 g/day) of tritium with a purity >95% is injected in the center of the WGTS beam tube with an inlet pressure of ≈10^{-3} mbar. In order to minimize systematic effects, the source tube inside the WGTS cryostat is cooled down to a temperature of ≈30 K. The beam tube temperature, the injection pressure, and the necessary gas throughput have to be kept stable on a level of <0.1% h^{-1} [17]. This is necessary as KATRIN uses a MAC-E filter [11,18] to scan the shape of the integral tritium β-spectrum. In contrast to the differential measurement of an energy spectrum, where all energies of the electrons are determined at the same time, the integral measurement determines the number of electrons with energies above the electrostatic retarding potential of the spectrometer. Moving through the energy region of interest step by step takes several hours. Fluctuations would lead to a distortion of the spectral shape.
- *Differential Pumping Section 1 (DPS1):* Connected on both sides to the WGTS beam tube are the first stages of the differential pumping section, the DPS1 (see Fig. 3). This section consists of 4 pump ports (PP) inside the WGTS cryostat (DPS1-F1, DPS1-F2, DPS1-R1, DPS1-R2) and one outside of it (PP0). A total of 14 turbomolecular pumps (TMP) of type Leybold MAG-W2800 with a pumping speed of 2100 ls^{-1} for H_2 [19] are connected to these pump ports. Twelve TMPs are arranged symmetrically around the WGTS beam tube, starting with 4 TMPs at each end, connected to DPS1-F1 and DPS1-R1. The next stage includes two TMPs in DPS1-F2 and DPS1-R2, respectively. The two remaining pumps are located at an additional pump port (PP0) between the WGTS cryostat and the DPS2 in downstream direction. The pump ports are connected via beam tube segments of 1 m length and a diameter of 90 mm.
  The fore-vacuum for the MAG-W2800 TMPs is provided by 4 Pfeiffer HiPace300 TMPs with a pumping speed of 220 ls^{-1} for

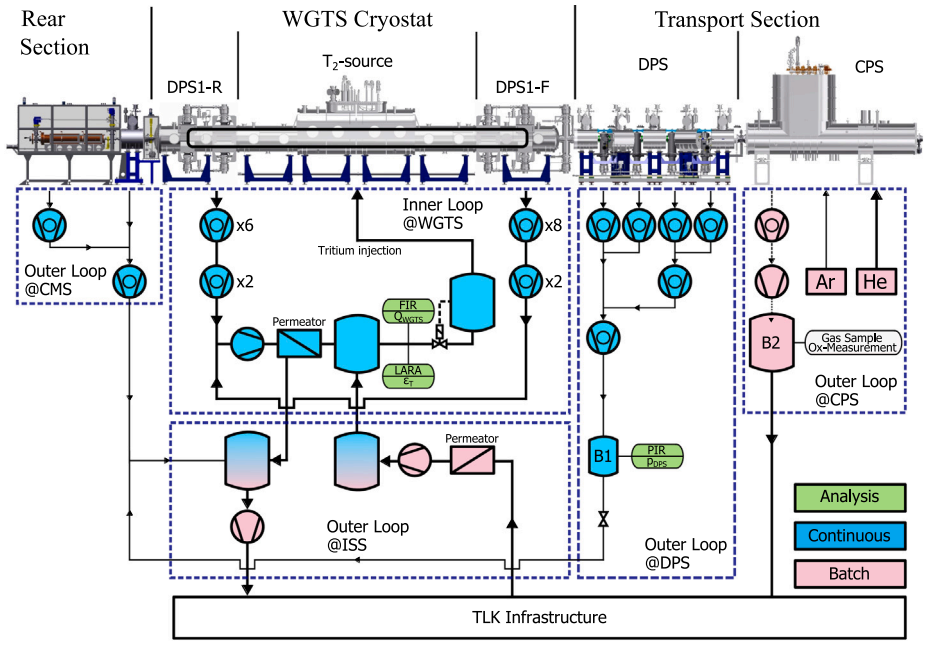

Fig. 2. Simplified flow diagram of the beamline and its pumps.

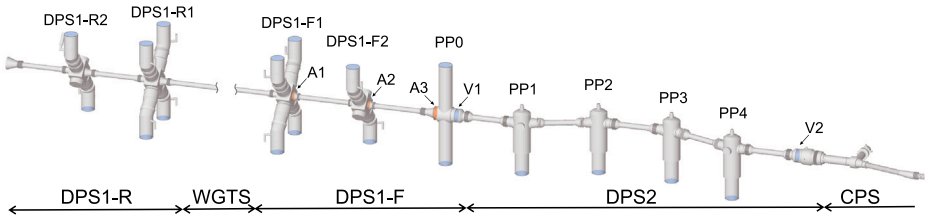

Fig. 3. Schematic drawing of the differential pumping section of the beam line. It shows only the beam tubes and the pump ports of the vacuum system, omitting the enclosing superconducting magnets and cryostats. The valve V1 separates the differential pumping sections connected to either the Inner Loop or the Outer Loop.

H_2 [20]. These pumps are in turn pumped by cascaded fore-pumps, combining a Normetex® scroll pump and a metal bellows pump [21] (see Fig. 2). Gas pumped out by this system is purified by a PdAg permeator and then re-injected into the WGTS (see [22] for details). The WGTS beam line and pump ports are part of the IL.

The pumps of the DPS1 reach an ultimate pressure of $<5 \times 10^{-10}$ mbar in the unbaked, 30 K cold WGTS cryostat, without gas load. When gas is circulating, the pumps reduce the gas flow towards the spectrometer by a factor of $\approx 10^3$, as is shown in Section 3.1.

- *Differential Pumping Section 2 (DPS2):* Separated from the DPS1 via a gate valve, four large, cascaded MAG-W2800 TMPs further reduce the downstream flow of neutral tritium in the DPS2 (PP1-4). The fore-vacuum for these pumps is provided by 2 Pfeiffer HiPace300 TMPs. Of these TMPs, the one pumping the PP3 and PP4 MAG-W2800 is cascaded with the other (see Fig. 2). The last HiPace300 TMP is in turn pumped by cascaded fore-pumps, combining a Normetex scroll pump and a metal bellows pump. In order to increase the pumping efficiency and prevent a direct line of sight between source and spectrometer, the DPS2 beam tube is arranged in a chicane (see Fig. 3. Gas pumped out from the DPS2 contains a high fraction of outgassing products, which decrease the purity of the tritium gas. Therefore, it is not re-circulated, but returned to the TLK infrastructure for purification. Hence, the DPS2 beam line and pump ports are part of the Outer Loop (OL).

  The pumps of the DPS2 reach an ultimate pressure of $<10^{-9}$ mbar in the unbaked system, without gas load. During gas circulation, the pumps reduce the gas flow towards the spectrometer by a factor of $\approx 10^4$, as is shown in Section 3.2.

- *Cryogenic Pumping Section (CPS):* Separated by another gate valve from the DPS2, about 2/3 of the CPS beamline is operated at a temperature of 3 K to 4 K, working as a cryo-pump for the remaining tritium. The inner surfaces of the cold beam tubes are enlarged by 90 circular fins welded into the beam tubes and covered by a layer of argon frost. Even with conservative assumptions, simulations indicate a reduction factor of at least 10^{11} [14], well above the minimum design value of 10^7. The performance of the CPS [23] is not covered in this paper, but it is used to determine the amount of tritium gas passing the DPS. During the regeneration of the cryo-surfaces the previously sorbed tritium, together with the argon frost, are evaporated and captured in a buffer vessel (B2). The activity of tritium in the gas is measured, allowing the determination of the total amount of tritium gas that passed the DPS.

The connections of the IL and OL to the infrastructure systems of the TLK are shown in Fig. 2.

2.2. Definition of reduction factor in existing setup

The overall reduction factor R_{tot} in the STS denotes the relative reduction of neutral tritium gas flow $Q_{\mathrm{WGTS,d}}$ from the WGTS to the spectrometers. R_{tot} needs to be larger than 10^{14}. It incorporates the reduction factors of the differential pumping sections R_{DPS} and of the cryogenic pumping section R_{CPS}, which are both required to reach at least a target value of 10^7:

$$R_{\mathrm{tot}} = R_{\mathrm{DPS}} \cdot R_{\mathrm{CPS}} \,. \tag{1}$$

In addition, R_{DPS} can be subdivided into reduction factors for the inner and outer loops, respectively:

$$R_{\mathrm{DPS}} = R_{\mathrm{IL}} \cdot R_{\mathrm{OL}}\,, \tag{2}$$

with:

- R_{IL} is the flow rate reduction between the downstream flow $Q_{\mathrm{WGTS,d}}$ from the injection point into the WGTS to the DPS2. This includes DPS1-F1, DPS1-F2, and PP0 up to V1, as shown in Fig. 3.
- R_{OL} is the flow rate reduction between the flow rate entering PP1 via A3 from the WGTS and the flow rate entering the CPS. In Fig. 3 this reduction factor is the fraction of gas entering the DPS2 through V1 over the gas exiting via V2.

In previous simulations [14,24] R_{DPS} was subdivided according to the different flow regimes, using laminar and transitional flow up to DPS1-F2 and molecular flow in PP0 and DPS2. However, for the measurements the reduction factors have to be split into R_{IL} and R_{OL}.

2.3. Results of simulations

The DPS1 is described in Ref. [24], which splits it into three computational domains. For the transition from the laminar flow regime at the injection point towards the transitional flow regime in the first pump ports, a semi-analytical rarefied gas dynamics model [25,26] is used. The transitional flow regime inside DPS1-F1 is simulated using a Direct Simulation Monte Carlo (DSMC) [27] method. Finally, the outermost pump ports are described, using the angular coefficient [28] method to account for the transition from 30 K to room temperature in this domain.

As the focus in [24] was on the precise description of the gas density distribution along the beamline, the reduction factor was not investigated in detail, and therefore no detailed error analysis was given. From the uncertainties given on the simulated pressures and flows, we estimate an uncertainty of about a factor two in both directions, mainly owing to the uncertainty of the effective pumping speed used in the simplified geometry of the model. The value for the gas flow reduction as reported in Ref. [24] is:

$$R^{\mathrm{Sim}}_{\mathrm{DPS1}} = 386^{+386}_{-193}\,. \tag{3}$$

In order to achieve comparability between measurement and simulation, the DPS2 MolFlow+ simulation performed in [14] has been rerun with slightly different boundary conditions, since the initial simulation included PP0 as part of the DPS2, while in the measurements it is connected to the IL.

MolFlow+ [28] is a Test Particle Monte Carlo (TPMC) simulation code for particle tracking through the geometry of a vacuum chamber in the molecular flow regime. Particles do not interact with each other but only with the walls of the vacuum chamber where they get adsorbed, desorbed or reflected. The geometry is approximated by a mesh of two-dimensional polygon surfaces, called facets. For each facet the number of hits, adsorptions and desorptions is counted. An adsorbing facet represents a pump, a desorbing facet a gas source. Fully transparent (virtual) facets which are not part of the actual physical geometry can be defined providing additional counting of hits at a location of interest. Ratios of counts are used in order to determine transmission probabilities. In Fig. 3 an overview of the implemented geometry is given. Besides the physical boundaries of the beam line there are several virtual facets implemented. The particle tracking starts at facet A2 downstream of DPS1-F2. Particles are removed from the simulation in three different cases: They

- hit facet A1,
- are pumped out by one of the TMPs in the pumping ports DPS1-F2 or PP0-4, or
- are pumped out at the CPS cryo-pump downstream of V2.

Table 1
Results of the DPS2 gas flow simulations with MolFlow+. Shown are the number of simulated test particles. Additionally, the numbers of particles terminated either at a group of TMPs or at the CPS cryo-pump are listed. These values are given for different TMP pumping probabilities α. For the number of particles entering PP0 via A3 (N_{A3}), back reflection through A3 towards DPS1-F2 has been taken into account by subtracting the hits of particles through A3 in upstream direction from the number of particles entering in downstream direction. This is equivalent to the total number of particles pumped by all adsorbing facets downstream of A3.

Particle tagged as	Notation	$\alpha = 0.20$	$\alpha = 0.25$	$\alpha = 0.30$
Total simulated particles		2.07×10^9	2.13×10^9	2.21×10^9
Entering PP0 via A3	N_{A3}	1.55×10^8	1.49×10^8	1.48×10^8
Pumped at PP0	N_{PP0}	1.43×10^8	1.39×10^8	1.39×10^8
Pumped at PP1-4	$N_{\mathrm{PP1-4}}$	1.16×10^7	1.02×10^7	9.42×10^6
Pumped at CPS	N_{CPS}	1.26×10^3	6.81×10^2	4.31×10^2

Consequently, the simulation does not only consist of the DPS2, but also the neighboring sections. Since particle tracking starts already at A2, while only facet counts at A3 and beyond are used in the simulation, it is assured, that boundary effects, such as back reflections or the angular distributions of particle velocities are included correctly. In MolFlow+ pumps are modeled by facets with well-defined sticking probabilities $\alpha \in [0, 1]$, corresponding to the pump's gas type dependent pumping probability. For the CPS cryo-pump $\alpha = 0.7$ was set, which is an established reference value of a well prepared argon layer at 3 K [29]. Particles moving as far back as DPS1-F1, hitting facet A1, are assumed to be pumped off. Consequently, these particles are removed from the simulation by setting $\alpha_{\mathrm{A1}} = 1$. It has been verified that this simplification of the model does affect the results of the simulation by less than 0.5%.

The DPS TMPs were included with $\alpha = 0.252$, corresponding to their estimated pumping probability for particles of mass $m = 6\,\mathrm{g\,mol^{-1}}$. For this estimate we used the nominal pumping speeds given by the manufacturer, interpolating different particle masses by applying the Malyshev model [30], which assumes that the pumping probability scales with the logarithm of the particle mass M ($\alpha \propto \ln(M)$). The systematic uncertainty of this method has been taken into account as an uncertainty of 20% on this pumping probability. It was estimated by comparing the measured and simulated pumping speeds for different gases (based on the nominal pumping speed of the pump manufacturer) in the KATRIN Main Spectrometer. The impact on the resulting reduction factor was obtained by dedicated simulations with 20% higher and 20% lower TMP pumping probabilities, respectively.

In Table 1 the output of the simulations is shown by giving the important numbers for the reduction factor calculations. Using the number of particles pumped at PP1-4 ($N_{\mathrm{PP1-4}}$) and at the CPS (N_{CPS}) for $\alpha = 0.25$ the resulting reduction factor is derived by the following equation:

$$R^{\mathrm{Sim}}_{\mathrm{OL}} = \frac{N_{\mathrm{PP1-4}}}{N_{\mathrm{CPS}}} = 1.50^{+0.69}_{-0.58} \times 10^4. \tag{4}$$

The upper and lower uncertainties originate from the simulations with $\alpha = 0.20$ and $\alpha = 0.30$ respectively. Since the maximal statistical uncertainty is about 4% and thus much smaller than the systematic uncertainty of about ≈40%, it is neglected in the following.

The reduction factor of the IL can be derived from $R^{\mathrm{Sim}}_{\mathrm{DPS1}}$ in Eq. (3) and the reduction factor of PP0. With the simulated numbers from Table 1, the reduction of the gas flow via PP0 is given by the ratio of particles entering PP0 through A3 (N_{A3}) and those pumped by the DPS2 ($N_{\mathrm{PP1-4}}$) and the CPS (N_{CPS}):

$$R^{\mathrm{Sim}}_{\mathrm{PP0}} = \frac{N_{\mathrm{A3}}}{N_{\mathrm{PP1-4}} + N_{\mathrm{CPS}}} = 1.460^{+0.110}_{-0.120} \times 10^1\,. \tag{5}$$

As for $R^{\mathrm{Sim}}_{\mathrm{DPS1}}$ however, there is one difference between the setup for which $R^{\mathrm{Sim}}_{\mathrm{DPS1}}$ was simulated and how it is operated in the current KATRIN setup. In [24] the simulation ended at the surface A3 with an assumed effective pumping probability of $\alpha = 20\%$ for PP0 and

the subsequent DPS2 pumps. This number originated from calculations for the case of only one active TMP at PP0. Currently, both TMPs are operated. So, the A3 effective pumping probability, as simulated with MolFlow+, should be rather 36% than 20%. The impact on the final result of $R^{\mathrm{Sim}}_{\mathrm{DPS1}}$ has been calculated based on two dedicated MolFlow+ simulations. In each of them A3 is assumed as an opaque facet but with different sticking factors of 20% and 36%, respectively. Gas particles are desorbed from facet A1. For both simulations the reduction factors have been calculated by taking the ratio of the number of adsorptions at A3 and hits at A2. The correction factor C_{A3} for $R^{\mathrm{Sim}}_{\mathrm{DPS1}}$ is determined as the ratio of both reduction factors, resulting in a value of $C_{\mathrm{A3}} = R_{36\%}/R_{20\%} = 0.953 \pm 0.003$. The corrected IL reduction factor is:

$$R^{\mathrm{Sim}}_{\mathrm{IL}} = C_{\mathrm{A3}} \cdot R^{\mathrm{Sim}}_{\mathrm{DPS1}} \cdot R^{\mathrm{Sim}}_{\mathrm{PP0}} = 5.4^{+6.2}_{-2.9} \times 10^{3} \,. \tag{6}$$

In combination with the simulated OL result from Eq. (4) one can derive the overall simulated reduction factor for the DPS:

$$R^{\mathrm{Sim}}_{\mathrm{DPS}} = R^{\mathrm{Sim}}_{\mathrm{IL}} \cdot R^{\mathrm{Sim}}_{\mathrm{OL}} = 8^{+17}_{-6} \times 10^{7} \,. \tag{7}$$

With the assumption that the uncertainties of the TMP pumping probabilities in DPS1 and DPS2 are correlated, the uncertainties were estimated using a maximum error approach. The upper and lower bounds given in Eq. (7) were obtained by subtracting the reduction factor values calculated for maximal ($\alpha = 0.30$) and minimal ($\alpha = 0.20$) pumping efficiency from the reduction factor calculated for the expected pumping probability of $\alpha = 0.25$.

3. Measurement of reduction factors

Two different methods were used to determine the reduction factors R_{IL} and R_{OL} for tritium. Measurements were taken for the nominal column density of $5.0 \times 10^{21}\,\mathrm{m^{-2}}$ ($\triangleq 100\%$) as well as for the settings used during the KNM1 ($1.1 \times 10^{21}\,\mathrm{m^{-2}} \triangleq 22\%$) and KNM2 ($4.2 \times 10^{21}\,\mathrm{m^{-2}} \triangleq 84\%$) measurement campaigns. While the reduction factor R_{IL} depends on the pressure in the WGTS beam tube and the temperature, R_{OL} is constant, since the DPS2 is operated at constant room temperature in the molecular flow regime. In contrast to the upper and lower bounds of uncertainty present for the theoretical results, the uncertainties for the derived quantities were calculated using uncertainty propagation assuming gaussian distributed uncertainties of the measured values. The different methods and their results are described below.

3.1. Reduction factor of the inner loop

The reduction factor R_{IL} is determined from the ratio of the measured gas flow rates into the WGTS and into the DPS2:

$$R_{\mathrm{IL}} = \frac{Q_{\mathrm{WGTS,d}}}{Q_{\mathrm{DPS2}}} \,. \tag{8}$$

The gas flow rate in downstream direction $Q_{\mathrm{WGTS,d}}$ inside the WGTS is determined using a MKS 179 mass flow meter[2] (labeled FIR in Fig. 2), which measures the total flow rate into the WGTS $Q_{\mathrm{WGTS,tot}}$. With the symmetric design of the WGTS beam tube and the DPS1-R and DPS1-F pump ports, equal conductances and effective pumping speeds in upstream and downstream direction can be assumed, leading to an equal split of the flow rate in both directions:

$$Q_{\mathrm{WGTS,d}} = \frac{1}{2} \cdot Q_{\mathrm{WGTS,tot}} \,. \tag{9}$$

The pressure ratio between the point of injection and both ends of the symmetrical sections, DPS1-F2 and DPS1-R2, is around 3 orders of magnitude. Therefore, the small effect of the difference in effective pumping speeds between the Rear Section at the upstream end and DPS2-PP0 at the downstream end can be neglected, compared to the systematic uncertainties of flow and pressure measurements which are on the percent-level.

Table 2
Results for the inner loop reduction factor measurements at different column densities. Given are the values for the gas flow rate from the center of the WGTS in downstream direction $Q_{\mathrm{WGTS,d}}$, fit results for the effective gas flow rate Q_{DPS2} entering the DPS2, as well as the Inner Loop reduction factors $R_{\mathrm{IL}} = Q_{\mathrm{WGTS,d}}/Q_{\mathrm{DPS2}}$. The identical uncertainties for $Q_{\mathrm{WGTS,d}}$ are due to the constant 1% F.S. accuracy of the flow meter. The uncertainty of Q_{DPS2} is dominated by the uncertainty of the buffer volume $\delta V_{\mathrm{B1}}/V_{\mathrm{B1}} = 1.3\%$. The uncertainties of the pressure measurements at the buffer vessel are 0.5%. For R_{IL} the errors are propagated in quadrature.

Column density $10^{21}\,\mathrm{m^{-2}}$	Temperature K	$Q_{\mathrm{WGTS,d}}$ mbar l $\mathrm{s^{-1}}$	Q_{DPS2} 10^{-4} mbar l $\mathrm{s^{-1}}$	R_{IL} 10^{3}
1.1	30	0.112 ± 0.017	0.293 ± 0.004	3.82 ± 0.58
1.8	80	0.256 ± 0.017	0.627 ± 0.009	4.09 ± 0.28
2.0	100	0.354 ± 0.017	0.782 ± 0.010	4.53 ± 0.22
4.2	30	0.756 ± 0.017	1.159 ± 0.015	6.52 ± 0.17
5.0	30	0.982 ± 0.017	1.471 ± 0.019	6.68 ± 0.14

The effective gas flow rate Q_{DPS2} entering the DPS2 is measured by a pressure rise $\Delta p/\Delta t$ inside the buffer vessel B1 (labeled PIR in Fig. 2) with a well known volume V_{B1}, located behind the last cascaded DPS2 TMP:

$$Q_{\mathrm{DPS2}} = V_{\mathrm{B1}} \cdot \frac{\Delta p}{\Delta t} \,. \tag{10}$$

The volume $V_{\mathrm{B1}} = (16.53 \pm 0.21)$ l has been determined during the commissioning phase via gas expansion from a reference volume. A necessary assumption for applying Eq. (10) is that all gas entering the DPS2 is pumped out by the 4 TMPs connected to the beamline, neglecting the gas entering the CPS. This assumption is justified, since the flow rate into the CPS is reduced by four orders of magnitude in the DPS2, which is much smaller compared to the systematic uncertainties for the flow and pressure measurement in the percent-level (see Section 3.2).

An additional effect is the outgassing of the DPS2 setup. The surfaces of the vacuum chambers, beam line instrumentation such as dipole electrodes or an ion monitor inside the vacuum system of the DPS2, as well as the TMPs themselves cause a non-negligible outgassing rate, leading to an additional pressure rise $\Delta p_{\mathrm{og}}/\Delta t_{\mathrm{og}}$ in V_{B1}. In order to correct for this effect, the outgassing rate was measured during operation of the beam line without tritium gas injection and then subtracted from the tritium gas flow induced pressure rise, which was measured using a MKS 722 capacitance diaphragm gauge[3]:

$$Q_{\mathrm{DPS2}} = V_{\mathrm{B1}} \cdot \left(\frac{\Delta p}{\Delta t} - \frac{\Delta p_{\mathrm{og}}}{\Delta t_{\mathrm{og}}} \right) \,. \tag{11}$$

The outgassing rate ($\approx 5 \times 10^{-7}$ mbar l $\mathrm{s^{-1}}$) is determined for each tritium measurement from the latest available outgassing measurement, in order to account for possible changes in the outgassing behavior. The pressure rise data and a linear fit for a column density of 5.0×10^{21} $\mathrm{m^{-2}}$ can be seen in Fig. 4. The results for Q_{DPS2}, $Q_{\mathrm{WGTS,d}}$, and R_{IL} for different column densities are listed in Table 2.

The monitoring of R_{IL} with reasonable accuracy has two direct applications for the operation of the source and transport section. First, with a constant R_{OL} the expected tritium load on the CPS is accessible with a measurement of R_{IL} on the time scale of 1 h to 2 h. This allows for reduction factor measurements to be done for different settings of WGTS cryostat temperatures and gas flows, which can change R_{IL}. Second, the fraction of gas which can be recirculated in the IL can be directly derived from this measurement. As such, R_{IL} has a direct impact on the operation of both the IL and OL.

[2] Full Scale (F.S.) of 200 sccm ($\approx$3.4 mbar l $\mathrm{s^{-1}}$), accuracy 1% of F.S., $\approx$2% at nominal column density.

[3] Full Scale (F.S.) of 26.6 mbar, accuracy 0.5% of rdg.

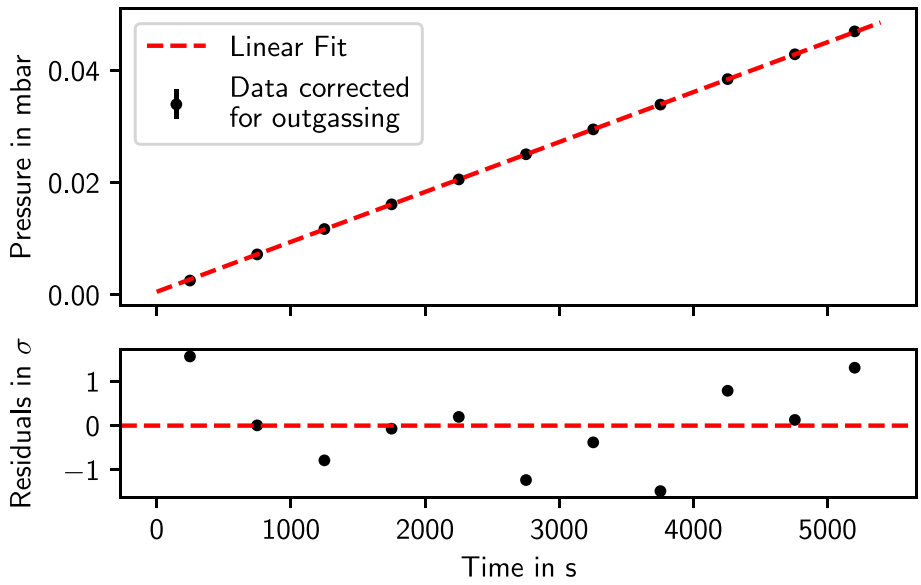

Fig. 4. Pressure in the buffer vessel B1 connected to the DPS2 TMPs vs. time. Shown as an example is the measurement with a column density of 5.0×10^{21} m^{-2}(≙ 100%). Measurements at other column densities show the same behavior with the only difference being the slope of the linear function. The outgassing rate was for all measurements about 5×10^{-7} mbar l s^{-1}, which is only 1% of Q_{DPS2} at 100% column density.

3.2. Reduction factor of the outer loop

The OL reduction factor R_{OL} is calculated in a two step process. First, a combined reduction factor $R_{\mathrm{DPS}} = R_{\mathrm{IL}} \cdot R_{\mathrm{OL}}$ is measured by comparing integral gas activities:

$$R_{\mathrm{DPS}} = \frac{A_{\mathrm{WGTS}}}{A_{\mathrm{CPS}}}\,. \tag{12}$$

where A_{WGTS} is the integral activity of beta-decays in the gas flow $Q_{\mathrm{WGTS,d}}$, and A_{CPS} is the beta-activity accumulated inside the CPS. The direct relation of the accumulated beta-activity to the integral gas flow into the CPS can be made, as isotopic exchange effects inside the DPS2 are expected to be on the sub-percent-level and therefore insignificant. This expectation is derived from the IL gas composition measurements for which gas passes through WGTS and DPS1, which are comparable to the DPS2 in length, the composition changes are below the percent-level for a single pass through.

To obtain R_{OL}, R_{DPS} is divided by R_{IL}:

$$R_{\mathrm{OL}} = \frac{R_{\mathrm{DPS}}}{R_{\mathrm{IL}}} = \frac{1}{R_{\mathrm{IL}}} \cdot \frac{A_{\mathrm{WGTS}}}{A_{\mathrm{CPS}}}\,. \tag{13}$$

This measurement method, using the activity of tritium gas, is needed as the cryogenic pumping principle of the CPS does not allow for an easily measurable gas accumulation in situ as described in Section 3.1. The gas flow entering the CPS is adsorbed on its cryogenic surface and can only be determined after regeneration. During the regeneration procedure, helium is used as a purge gas to remove the argon frost layer together with the captured tritium. This results in a mixture of around ~6 bar l argon, 250 bar l helium, and traces of tritium of less than 0.39 mbar l, limited by the maximum allowed activity inside the CPS. The entire gas is collected in the buffer vessel B2 (see Fig. 2). Reliable quantification of the small trace amounts of tritium in this gas mixture is impossible using pressure measurements and very challenging using residual gas analyzers. However, the traces of tritium are quantifiable by counting the beta-activity in the gas with measurement techniques developed by TLK [31–33].

Several samples of this gas mixture from the buffer vessel were analyzed, using oxidation on copper oxide (CuO) at 450 °C, followed by liquid scintillation counting to determine the activity concentration of the gas sample with an uncertainty of 10%. The total activity of the collected purge gas A_{CPS} was calculated by scaling the sample activity with the respective gas amounts.

Table 3
Results for the combined reduction factor R_{DPS} measurements during the KNM1 and KNM2 measurement campaigns. Given are the values for integral beta-activity A_{WGTS} of the WGTS downstream gas flow $Q_{\mathrm{WGTS,d}}$, the total accumulated beta-activity on the CPS A_{CPS}, the combined reduction factor R_{DPS} as well as the Outer Loop reduction factor $R_{\mathrm{OL}} = A_{\mathrm{WGTS}} \cdot A_{\mathrm{CPS}}^{-1} \cdot R_{\mathrm{IL}}^{-1}$ derived using the Inner Loop reduction factors R_{IL} from Table 2.

Measurement campaign	A_{WGTS} in 10^{17} Bq	A_{CPS} in 10^{9} Bq	R_{DPS} in 10^{7}	R_{OL} in 10^{4}
KNM1	0.94 ± 0.13	1.56 ± 0.16	6.04 ± 1.03	1.58 ± 0.36
KNM2	4.10 ± 0.12	4.26 ± 0.43	9.63 ± 1.00	1.48 ± 0.16

The determination of the activity A_{WGTS} is not possible via a direct activity measurement. It can be derived from the gas flow $Q_{\mathrm{WGTS,d}}$ and the composition of the gas. The gas composition is measured via laser raman spectroscopy [34–36]. The composition analysis allows the determination of the fraction of tritium ϵ_{T}. Using these two values and the specific activity $a_{\mathrm{T}_2} = 9.5 \times 10^{10}$ Bq/mbar l of T_2, one can calculate the integral activity A_{WGTS} as follows:

$$A_{\mathrm{WGTS}} = a_{\mathrm{T}_2} \cdot \int Q_{\mathrm{WGTS,d}}(t) \cdot \epsilon_{\mathrm{T}}(t)\mathrm{d}t\,. \tag{14}$$

The measurement results for A_{WGTS} and A_{CPS} for the CPS regenerations after the KNM1 and KNM2 measurement campaigns, as well as the reduction factors R_{DPS} and R_{OL}, are shown in Table 3.

4. Discussion

4.1. Inner loop reduction factor

The simulated IL reduction factor for the nominal column density of 5×10^{21} m^{-2}(≙ 100%) as derived in this work (see Section 2.3) is:

$$R_{\mathrm{IL}}^{\mathrm{Sim}} = 5.4^{+6.2}_{-2.9} \times 10^{3}. \tag{15}$$

Comparing this to the measured value of the IL reduction factor,

$$R_{\mathrm{IL}} = (6.68 \pm 0.14) \times 10^{3}, \tag{16}$$

one can see that the reduction factor expected from the simulation and the assumed pumping probability of $\alpha = 0.25$, could nicely be confirmed by measurements.

An effect which had not been expected initially, is the significantly different reduction factor at the low column density setting of $1.1 \times 10^{21}\,\mathrm{m}^{-2}(\approxeq 22\%)$ used during KNM1 (see Table 2). This strong dependence of the reduction factor on the column density, and thereby pressure and flow, can be attributed to the changes of flow regime inside the WGTS. With decreasing column density, the pressure inside the pump ports decreases, shifting the flow regime from the Knudsen flow regime further towards the free molecular flow regime. In the Knudsen flow regime more scattering of gas molecules inside the DPS1-F1 is present. The narrow and long geometry of the beam line between the injection point and DPS1-F1 produces a distinct molecular beam. Thus, radial movement is suppressed and molecules only receive a strong radial momentum by scattering with other molecules. Since gas particles are only pumped if they move radially towards the TMPs, less scattering produces lower reduction factors. This effect is the most likely reason for the smaller reduction factors of the IL at low column densities. Various measurements of R_{IL} at different column densities and beam line temperatures showed that there is no strong influence of the temperature, but a clear correlation with the column density (see Table 2). As the DSMC simulations for the Knudsen flow regime are computationally intensive, and low column densities are not of interest for normal KATRIN operation, a detailed parameter study was not undertaken.

4.2. Outer loop reduction factor

The simulated OL reduction factor, as derived in this work (see Section 2.3), is:

$$R_{\mathrm{OL}}^{\mathrm{Sim}} = 1.50^{+0.69}_{-0.58} \times 10^{4}. \tag{17}$$

Comparing this to the value of the OL reduction factor derived in the KNM2 measurement campaign,

$$R_{\mathrm{OL}} = (1.48 \pm 0.16) \times 10^{4}, \tag{18}$$

one can see that the values match well within their respective uncertainties. In contrast to R_{IL}, no dependence of R_{OL} on the column density can be inferred from the data, considering the measurement uncertainties. This is in good agreement with the underlying assumption of free molecular flow inside the OL section of the differential pumping section.

4.3. Impact of the reduction factor on CPS operation

While there is no data on the combined reduction factor for the differential pumping sections R_{DPS} at nominal column density of $5 \times 10^{21}\,\mathrm{m}^{-2}$, an estimation can be made using the data gained from KNM2 with a column density of $4.2 \times 10^{21}\,\mathrm{m}^{-2}$. The difference between R_{IL} for both column densities is negligible, and R_{OL} does not depend on the column density value. As such, the R_{DPS} measured during KNM2,

$$R_{\mathrm{DPS}} = (9.63 \pm 1.00) \times 10^{7}\,, \tag{19}$$

can be used as a good estimate for the reduction factor at nominal conditions, which is very promising with regards to the CPS runtime. The runtime of the CPS is limited by the maximal allowed amount of $N_{\mathrm{CPS,max}} = 0.39$ mbar l ($\hat{=}\,1$ Ci) of accumulated tritium gas. At the nominal tritium gas flow rate of $Q_{\mathrm{WGTS,d}} = 0.98$ mbar l s^{-1} from the point of injection in downstream direction, this leads to a maximum operation time before regeneration of:

$$t_{\mathrm{CPS,max}} = \frac{N_{\mathrm{CPS,max}}}{Q_{\mathrm{WGTS,d}}} \cdot R_{\mathrm{DPS}} = (445 \pm 46)\,\mathrm{days}\,. \tag{20}$$

This value surpasses the initial design goal of a CPS regeneration every 60 days by a factor of 7.4. With this rather large safety margin, the measurement interval between subsequent regenerations can be relaxed, allowing for longer neutrino mass runs, and more flexibility in scheduling of measurements in general.

5. Summary and conclusion

The KATRIN experiment requires a reduction of the tritium flow in the beamline between the point of injection in the WGTS and the spectrometer and detector section by at least 14 orders of magnitude. Otherwise, the additional background rate would worsen the ultimate sensitivity for the neutrino mass. The huge gas flow reduction is achieved by two sequential pumping systems, each reducing the flow by a factor of at least 10^7, using turbo-molecular pumps (DPS) and cryosorption on 3 K cold argon frost (CPS), respectively.

For the initial design layout, radiation safety considerations required a regeneration of the cryogenic pumping section after no more than 60 days. A sound knowledge of the actual reduction factor of the DPS allows for a more accurate estimate of the time interval between regenerations, helping to optimize the time available for neutrino mass measurements.

Therefore, extensive gas flow simulations were performed, taking into account the different flow regimes along the beamline, from laminar and transitional flow to molecular flow. The simulation of the DPS resulted in a reduction factor of $8^{+17}_{-6} \times 10^{7}$, well above the minimum requirement.

To validate the simulations, the tritium reduction factor of the differential pumping sections was measured for the first time in 2019 for different flow rates, with a tritium purity well above 97%.

The measured value for a tritium column density of $4.2 \times 10^{21}\,\mathrm{m}^{-2}$ in the beamtube of the WGTS is $R_{\mathrm{DPS}} = (9.63 \pm 1.00) \times 10^{7}$. This reduction factor, measured at 84% of the nominal column density, as used during the most recent neutrino runs, is well above the minimum requirement of 10^7 and is in good agreement with the simulated value.

In conclusion, the good performance of the final design of the differential pumping section of the KATRIN experiment could be demonstrated both by simulation and measurement for the first time. This performance allows the long-term operation of the cryogenic pumping section as intended, enabling the KATRIN experiment to accumulate the necessary amount of measurement runs for its scientific goals.

Declaration of competing interest

The authors declare that they have no known competing financial interests or personal relationships that could have appeared to influence the work reported in this paper.

Acknowledgments

We acknowledge the support of the Helmholtz Association (HGF), Germany, the German Ministry for Education and Research BMBF (05A17VK2), DFG graduate school KSETA, Germany (GSC 1085), and the Research Training Group, Germany (GRK1694).

We would like to thank Jochen Bonn, Burkhardt Freudiger and Oleg Kazachenko for their ideas and valuable contributions on concepts and design of the experiment and Woosik Gil for his support with the magnet systems and questions related to magnetic fields. We would furthermore like to thank Tobias Falke, David Hillesheimer, Joschua Kopheiss, Saskia Schäfer, and Tobias Weber for their help in operation of the TLK infrastructure as well as laboratory analyses. Last but not least we would like to thank Valery Popov and Jörg Brandt for their contributions to the design and construction of the beam line setup as well as Norbert Kernert for his valuable contributions for the setting up and commissioning of the vacuum components and the tritium loops.

References

[1] Z. Zeng, S. Yeung, M. chung Chu, Effects of neutrino mass and asymmetry on cosmological structure formation, J. Cosmol. Astropart. Phys. 2019 (03) (2019) 015, http://dx.doi.org/10.1088/1475-7516/2019/03/015.

[2] Y. Fukuda, T. Hayakawa, E. Ichihara, K. Inoue, et al., Evidence for oscillation of atmospheric neutrinos, Phys. Rev. Lett. 81 (8) (1998) 1562–1567, http://dx.doi.org/10.1103/physrevlett.81.1562.

[3] E.D. Valentino, E. Giusarma, M. Lattanzi, O. Mena, et al., Cosmological axion and neutrino mass constraints from planck 2015 temperature and polarization data, Phys. Lett. B 752 (2016) 182–185, http://dx.doi.org/10.1016/j.physletb.2015.11.025.

[4] M. Tanabashi, K. Hagiwara, K. Hikasa, K. Nakamura, Y. Sumino, et al., Review of particle physics, Phys. Rev. D 98 (3) (2018) http://dx.doi.org/10.1103/physrevd.98.030001.

[5] M. Aker, K. Altenmüller, M. Arenz, M. Babutzka, et al., Improved upper limit on the neutrino mass from a direct kinematic method by KATRIN, Phys. Rev. Lett. 123 (22) (2019) http://dx.doi.org/10.1103/physrevlett.123.221802.

[6] P. de Salas, D. Forero, C. Ternes, M. Tórtola, J. Valle, Status of neutrino oscillations 2018: 3σ hint for normal mass ordering and improved CP sensitivity, Phys. Lett. B 782 (2018) 633–640, http://dx.doi.org/10.1016/j.physletb.2018.06.019.

[7] KATRIN collaboration, KATRIN design report (7090), 2005, URL http://bibliothek.fzk.de/zb/berichte/FZKA7090.pdf.

[8] M. Arenz, W.-J. Baek, M. Beck, A. Beglarian, et al., First transmission of electrons and ions through the KATRIN beamline, J. Instrum. 13 (04) (2018) P04020, http://dx.doi.org/10.1088/1748-0221/13/04/p04020.

[9] M. Aker, K. Altenmüller, M. Arenz, W.-J. Baek, et al., First operation of the KATRIN experiment with tritium, Eur. Phys. J. C 80 (3) (2020) http://dx.doi.org/10.1140/epjc/s10052-020-7718-z.

[10] M. Arenz, M. Babutzka, M. Bahr, J. Barrett, et al., Commissioning of the vacuum system of the KATRIN main spectrometer, J. Instrum. 11 (2016) P04011, http://dx.doi.org/10.1088/1748-0221/11/04/P04011, arXiv:1603.01014.

[11] A. Picard, H. Backe, H. Barth, J. Bonn, B. Degen, et al., A solenoid retarding spectrometer with high resolution and transmission for keV electrons, Nucl. Instrum. Methods Phys. Res. B 63 (3) (1992) 345–358, http://dx.doi.org/10.1016/0168-583x(92)95119-c.

[12] W. Gil, J. Bonn, B. Bornschein, R. Gehring, et al., The cryogenic pumping section of the KATRIN experiment, IEEE Trans. Appl. Supercond. 20 (3) (2010) 316–319, http://dx.doi.org/10.1109/tasc.2009.2038581.

[13] C. Röttele, Results of the first cool-down of the KATRIN cryogenic pumping section, J. Phys. Conf. Ser. 888 (2017) 012228, http://dx.doi.org/10.1088/1742-6596/888/1/012228.

[14] F. Friedel, C. Röttele, L. Schimpf, J. Wolf, et al., Time-dependent simulation of the flow reduction of D2 and T2 in the KATRIN experiment, Vacuum 159 (2019) 161–172, http://dx.doi.org/10.1016/j.vacuum.2018.10.002.

[15] F. Priester, M. Sturm, B. Bornschein, Commissioning and detailed results of KATRIN inner loop tritium processing system at tritium laboratory karlsruhe, Vacuum 116 (2015) 42–47, http://dx.doi.org/10.1016/j.vacuum.2015.02.030.

[16] S. Welte, M. Sturm, D. Hillesheimer, L.T. Le, S. Schäfer, E. Fanghänel, F. Priester, A. Marsteller, Tritium supply and processing for the first KATRIN tritium operation, Fusion Sci. Technol. (2020) 1–5, http://dx.doi.org/10.1080/15361055.2019.1705681.

[17] M. Babutzka, M. Bahr, J. Bonn, B. Bornschein, A. Dieter, et al., Monitoring of the operating parameters of the KATRIN windowless gaseous tritium source, New J. Phys. 14 (10) (2012) 103046, http://dx.doi.org/10.1088/1367-2630/14/10/103046.

[18] V. Lobashev, P. Spivak, A method for measuring the electron antineutrino rest mass, Nucl. Instrum. Methods Phys. Res. A 240 (2) (1985) 305–310, http://dx.doi.org/10.1016/0168-90028590640-0.

[19] Leybold Vacuum, Operating instructions MAGdigital series, GA 05.141/5.02, 2002.

[20] Pfeiffer Vacuum, Operating instructions HiPace300 turbopump, PT 0200 BEN/I (1603), 2016.

[21] M.H. Chang, S. Cho, J.Y. Lim, S.B. Kang, M.K. Lee, et al., Performance test of pump combination between normetex 15 scroll and MB 601 pumps, Fusion Sci. Technol. 60 (3) (2011) 918–921, http://dx.doi.org/10.13182/fst11-a12566.

[22] F. Priester, D. Hillesheimer, A. Marsteller, M. Röllig, M. Sturm, Tritium processing systems and first tritium operation of the KATRIN experiment, Fusion Sci. Technol. (2020) 1–5, http://dx.doi.org/10.1080/15361055.2020.1730118.

[23] C. Röttele, Tritium Suppression Factor of the Katrin Transport Section, (Ph.D. thesis), Karlsruhe Institute of Technology (KIT, 2019, http://dx.doi.org/10.5445/IR/1000096733.

[24] L. Kuckert, F. Heizmann, G. Drexlin, F. Glück, et al., Modelling of gas dynamical properties of the KATRIN tritium source and implications for the neutrino mass measurement, Vacuum 158 (2018) 195–205, http://dx.doi.org/10.1016/j.vacuum.2018.09.036.

[25] F. Sharipov, Rarefied Gas Dynamics, Wiley-VCH Verlag GmbH & Co. KGaA, 2016, http://dx.doi.org/10.1002/9783527685523.

[26] F. Sharipov, Rarefied gas flow through a long tube at arbitrary pressure and temperature drops, J. Vac. Sci. Technol. A 15 (4) (1997) 2434–2436, http://dx.doi.org/10.1116/1.580904.

[27] G.A. Bird, Molecular Gas Dynamics and the Direct Simulation of Gas Flows, Oxford University Press, Oxford, 1994.

[28] R. Kersevan, J.-L. Pons, Introduction to MOLFLOW+: New graphical processing unit-based Monte Carlo code for simulating molecular flows and for calculating angular coefficients in the compute unified device architecture environment, J. Vac. Sci. Technol. A 27 (4) (2009) 1017–1023, http://dx.doi.org/10.1116/1.3153280.

[29] V.B. Yuferov, P.M. Kobzev, Investigation of cryosorption extraction of Helium, Hydrogen, and Deuterium by layers of condensed gases, Sov. Phys. Tech. Phys. 14 (1970) 1261.

[30] O.B. Malyshev, Characterisation of a turbo-molecular pumps by a minimum of parameters, Vacuum 81 (6) (2007) 752–758, http://dx.doi.org/10.1016/j.vacuum.2005.11.055.

[31] D. Corneli, B. Bornschein, E. Fanghänel, M. Glugla, et al., Memory effects in measurements of low tritium concentrations as required for the outlet of the TEP system of the ITER fuel cycle, Fusion Sci. Technol. 48 (1) (2005) 55–58, http://dx.doi.org/10.13182/fst05-a879.

[32] M. Röllig, S. Ebenhöch, S. Niemes, F. Priester, M. Sturm, Development of a compact tritium activity monitor and first tritium measurements, Fusion Eng. Des. 100 (2015) 177–180, http://dx.doi.org/10.1016/j.fusengdes.2015.05.056.

[33] S. Ebenhöch, S. Niemes, F. Priester, M. Röllig, Investigations of the applicability of a new accountancy tool in a closed tritium loop, Fusion Eng. Des. 109-111 (2016) 1376–1379, http://dx.doi.org/10.1016/j.fusengdes.2015.12.018.

[34] M. Sturm, M. Schlösser, R.J. Lewis, B. Bornschein, et al., Monitoring of all hydrogen isotopologues at Tritium laboratoryKarlsruhe using Raman spectroscopy, Laser Phys. 20 (2) (2009) 493–507, http://dx.doi.org/10.1134/s1054660x10030163.

[35] M. Schlösser, S. Rupp, H. Seitz, S. Fischer, et al., Accurate calibration of the laser Raman system for the Karlsruhe Tritium neutrino experiment, J. Mol. Struct. 1044 (2013) 61–66, http://dx.doi.org/10.1016/j.molstruc.2012.11.022.

[36] M. Aker, K. Altenmüller, A. Beglarian, J. Behrens, A. Berlev, et al., Quantitative long-term monitoring of the circulating gases in the KATRIN experiment using raman spectroscopy, Sensors 20 (17) (2020) 4827, http://dx.doi.org/10.3390/s20174827.

Glossary

CMS: Calibration and Monitoring Section
CPS: Cryogenic Pumping Section
DPS: Differential Pumping Section
DPS1: First stage of the differential pumping section consisting of DPS1-R, DPS1-F, and PP0
DPS2: Second stage of the differential pumping section consisting of PP1-PP4
DPS1-R: DPS1 pump ports situated inside the WGTS cryostat in rearward direction
DPS1-F: DPS1 pump ports situated inside the WGTS cryostat in forward direction
DPS1-R1: First DPS1 pump port in rearward direction
DPS1-F1: First DPS1 pump port in forward direction
DPS1-R2: Second DPS1 pump port in rearward direction
DPS1-F2: Second DPS1 pump port in forward direction
IL: The "Inner Loop" of the tritium loops system responsible for direct recirculation through the WGTS
KATRIN: KArlsruhe TRItium Neutrino experiment
KNM1: First KATRIN neutrino mass measurement campaign
KNM2: Second KATRIN neutrino mass measurement campaign
MAC-E: filter Magnetic Adiabatic Collimation with Electrostatic filter
OL: The "Outer Loop" of the tritium loops system responsible for gas flow reduction towards the SDS and exhaust gas collection
PP0: An additional pump port belonging to the DPS1 which is situated outside the WGTS cryostat
PP1-4: The four pump ports of the DPS2
TLK: Tritium Laboratory Karlsruhe
SDS: Spectrometer and Detector Section
STS: Source and Transport Section
WGTS: Windowless Gaseous Tritium Source